Karen M. Assmann · Ralph Timmermann

Variability of dense water formation in the Ross Sea

Abstract This paper presents results from a model study of the interannual variability of high salinity shelf water (HSSW) properties in the Ross Sea. Salinity and potential temperature of HSSW formed in the western Ross Sea show oscillatory behaviour at periods of 5–6 and 9 years superimposed on long-term fluctuations. While the shorter oscillations are induced by wind variability, variability on the scale of decades appears to be related to air temperature fluctuations. At least part of the strong decrease of HSSW salinities deduced from observations for the period 1963–2000 is shown to be an aliasing artefact due to an undersampling of the periodic signal. While sea ice formation is responsible for the yearly salinity increase that triggers the formation of HSSW, interannual variability of net freezing rates hardly affects changes in the properties of the resulting water mass. Instead, results from model experiments indicate that the interannual variability of dense water characteristics is predominantly controlled by variations in the shelf inflow through a sub-surface salinity and a deep temperature signal. The origin of the variability of inflow characteristics to the Ross Sea continental shelf can be traced into the Amundsen and Bellingshausen Seas. The temperature anomalies are induced at the continental shelf break in the western Bellingshausen Sea by fluctuations of the meridional transport of circumpolar deep water with the eastern cell of the Ross Gyre. In the Amundsen Sea, upwelling due to a persistently cyclonic wind field carries the signal into the surface mixed layer, leading to fluctuations of the vertical heat flux, anomalies of brine release near the sea ice edge, and consequently to a sub-surface salinity anomaly. With the westward flowing coastal current, both the sub-surface salinity and deep temperature signals are advected onto the Ross Sea continental shelf. Convection carries the signal of salinity variability into the deep ocean, where it interacts with modified circumpolar deep water upwelled onto the continental shelf as the second source water mass of HSSW. Sea ice formation on the Ross Sea continental shelf thus drives the vertical propagation of the signal rather than determining the signal itself.

Keywords Numerical modelling · BRIOS ·
Ross Sea · Amundsen Sea · Interannual variability ·
High salinity shelf water (HSSW)

K. M. Assmann · R. Timmermann
Alfred Wegener Institute for Polar and Marine Research,
Bussestr. 24, 27570 Bremerhaven, Germany

Present address: K. M. Assmann (✉)
Bjerknes Centre for Climate Research,
Allégalen 55, 5007 Bergen, Norway
E-mail: karen.assmann@bjerknes.uib.no
Tel.: +47-555 83709
Fax: +47-555 89883

1 Introduction

Stratification of the lower- and mid-latitude oceans is usually stable with warmer, and hence lighter, surface waters overlying a large volume of colder, denser deep and bottom waters. Exchange between these regimes and ventilation of the deep and bottom layers occurs in the polar oceans, e.g. the Greenland Sea in the Arctic and the Antarctic continental shelves. Cold, saline shelf waters are formed during winter and evolve into Antarctic Bottom Water after mixing with modified forms of Circumpolar Deep Water during their descent down the continental slope (Foster and Carmack 1976). This process is mainly driven by vigorous sea ice formation in coastal polynyas, which are kept ice free by consistently strong offshore winds descending from the continental plateau. The associated brine release leads to instability of the weakly stratified water column and hence to deep convection and vertical mixing.

In the western Ross Sea (Fig. 1) sea ice is driven northward by persistent, strong southerly winds descending from the Transantarctic Mountains of Victoria Land (Jacobs and Comiso 1989). During autumn and winter this results in vigorous brine release and

allows for the formation of high salinity shelf water (HSSW), the densest water mass found anywhere on the Antarctic continental shelf (Jacobs et al. 1970; Jacobs and Giulivi 1998; Assmann et al. 2003).

The Ross Sea continental shelf, generally ice-free during the summer months, is among the most densely sampled regions in the Antarctic marginal seas. Observations are available for the past four decades (Jacobs and Giulivi 1998). Jacobs et al. (2002) used the available database to identify a freshening trend in the Ross Sea HSSW salinities whose origin they hypothesize to lie in changes in the upstream regions.

The main inflow to the Ross Sea continental shelf is formed by the Ross Gyre's southern branch, which follows the coastal easterly winds. However, detailed knowledge of ocean circulation and properties of the upstream region, i.e. the Amundsen and Bellingshausen Seas, is sparse due to the thick perennial sea ice cover in this region (Heap 1964; Jeffries et al. 1998) and the fact that the water mass characteristics make the Amundsen and Bellingshausen Sea an unlikely site for bottom water formation (Hellmer et al. 1998; Baines and Condie 1998).

This work presents a numerical model investigation of the factors affecting dense water formation on the Ross Sea continental shelf and their variability. It aims to establish links between the Ross Sea continental shelf as the dense water formation site and the Amundsen and Bellingshausen Seas as source regions of water masses entering the Ross Sea continental shelf.

The paper is organised as follows: a description of the coupled ice-ocean model used is followed by a brief introduction to the mean circulation pattern in the Pacific sector of the Southern Ocean which is also used for model evaluation. We then present the interannual variability of dense water properties on the Ross Sea continental shelf as represented by the numerical model and compare it to observations. The influence of atmospheric forcing on the interannual variability of the local fresh water fluxes is analysed. The inflow variability to the Ross Sea continental shelf is investigated as an external source for the interannual variability of shelf water characteristics. The investigation closes by identifying processes in the Amundsen and Bellingshausen Seas that may determine the inflow characteristics to the Ross continental shelf.

2 Model description

The coupled sea ice–ice shelf–ocean model BRIOS-2.2 employed here has been previously applied to the Weddell and Ross Seas (Timmermann et al. 2002a, b; Assmann et al. 2003). The ocean component is based on the S-coordinate primitive equation model SPEM (Haidvogel et al. 1991), and the sea ice component on a dynamic-thermodynamic sea ice model with viscous-plastic rheology (Hibler 1979). In the ocean, the Pacanowski and Philander (1981) mixing scheme ensures that vertical mixing is continuously increased for a weakening stratification and increasing vertical shear. The vertical diffusivity was given an upper limit of 10^{-2} m^2 s^{-1}. For sea ice, the Parkinson and Washington (1979) thermodynamics are employed, using the Semtner (1976) zero-layer approach for heat conduction. Inclusion of a prognostic snow layer (Owens and Lemke 1990) accounts for the effect of flooding (Leppäranta 1983; Fischer 1995). The model domain includes the larger ice shelf cavities (Fig. 1) and the exchange of heat and fresh water between ice shelf and ocean at the ice shelf base. Interactions between ice shelf base and ocean are treated the same way as between sea ice and ocean, whereby the freezing point temperature is calculated as a function of pressure and salinity for the whole model domain. Ice shelf extent and thickness are prescribed as

Fig. 1 Model representation of bottom topography for the Southeast Pacific sector derived from Smith and Sandwell (1997) and ETOPO5 (south of 72°S). *CA* Cape Adare, *AI* Alexander Island, *BI* Balleny Islands Plateau, *CSI* Carney and Siple Islands, *RI* Ross Island, *RvI* Roosevelt Island, *TI* Thurston Island
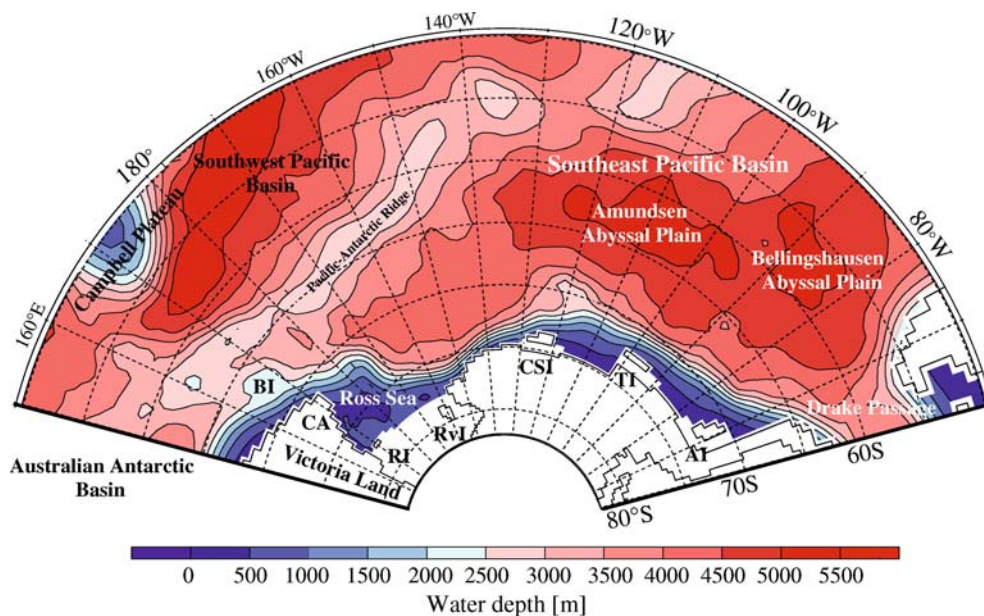
constant over time, and ice velocities are set to zero (Timmermann et al. 2002a).

The model is run on a circumpolar grid with zonal boundaries at 48°S and 82°S, an isotropic resolution of 1.5° zonally and 1.5°cos(ϕ) meridionally for the whole model domain, and 24 vertical levels with increasing resolution near surface and bottom. Bottom topography is from Smith and Sandwell (1997) north of 72°S, and ETOPO5 data south of 72°S. Ice shelf and water column thicknesses for the large ice shelf cavities are from Greischar et al. (1992) (Ross) and Johnson and Smith (1997) (Filchner-Ronne). Ice shelf thickness is set to 200 m for the smaller ice shelves, George VI, Abbot and Getz in the South East Pacific.

The hydrographic data for initialization and restoring at the northern boundary are from the WOCE Hydrographic Programme Special Analysis Centre (Gouretski et al. 1999). Along the northern model boundary, temperature and salinity are nudged towards this climatology over a strip five grid cells wide using a linear damping term with decreasing time scale towards the boundary. No other flux corrections or restoring to observed distributions are used. Since the Antarctic Circumpolar Current is not fully included in the model domain, assumptions have to be made about its course at 50°S. As in Timmermann et al. (2002a) and Beckmann et al. (1999), transport through Drake Passage is set to 130 Sv (Whitworth and Peterson 1985). Half of this is extracted from the model domain between the east coast of South America and 30°W, and reintroduced between 120°E and 180° in the Indian Sector.

For atmospheric forcing, daily NCEP Reanalyses for 10-m wind speed, 2-m air temperature, specific humidity, cloudiness, and net precipitation (P-E) are used for the period from 1948 to 2001. The period from 1948 to 1957 was used as spin-up time for the model while the years 1958 to 2001 were used for analysis.

3 Simulated basin-scale circulation

A thorough evaluation of the model's ability to produce a realistic represention of water mass distribution and circulation on the Ross Sea continental shelf was performed by Assmann et al. (2003). Here, we concentrate on the larger-scale characteristics of the simulated ocean circulation in the Ross, Amundsen and Bellingshausen Seas.

Similar to the Weddell Sea the basin north of the Ross Sea continental shelf is occupied by a large cyclonic gyre (Fig. 2). In contrast to the Weddell Gyre its transport and structure are largely unknown except for a few estimates (e.g. Locarnini 1994; Gouretski 1999). In the coupled ice-ocean model BRIOS-2.2 the Ross Gyre shows a double-cell structure like the Weddell Gyre (Beckmann et al. 1999). However, rather than having two cells of approximately equal transport, the western cell of the Ross Gyre with a maximum of ~20 Sv is twice as strong as its eastern counterpart (9 Sv). In the Pacific sector the ACC is steered southward through fracture zones in the Pacific-Antarctic Ridge which forms the northwestern boundary of the gyre. This intrusion leads to the asymmetry in transport strength of the gyre's cells and to the presence of relatively warm CDW much further south in the Southeast Pacific than in the Weddell Sea (Orsi et al. 1995; Hellmer et al. 1998). Henceforth, we will refer to the western cell as the Ross Gyre and the eastern as the Ross Gyre extension.

While the western end of the gyre is clearly defined by the Balleny Island plateau at 170°E (Botnikov and Chuguy 1989; Gouretski 1999), opinions about the location of the eastern boundary vary ranging from 125°W (Reid 1986; Botnikov and Chuguy 1989) to 140°W (Locarnini 1994; Gouretski 1999). The model identifies 130°W as the eastern boundary for the main, western cell, while strictly

Fig. 2 Vertically integrated transport from BRIOS–2.2 in the Pacific sector of the Southern Ocean. Long-term mean of the simulated barotropic stream function ψ. Isolines for negative values are *dashed* with a contour interval of 5 Sv, *solid ones* for positive values have a contour interval of 2 Sv and are *colour-coded*. Positive features in the stream function are associated with a cyclonic circulation
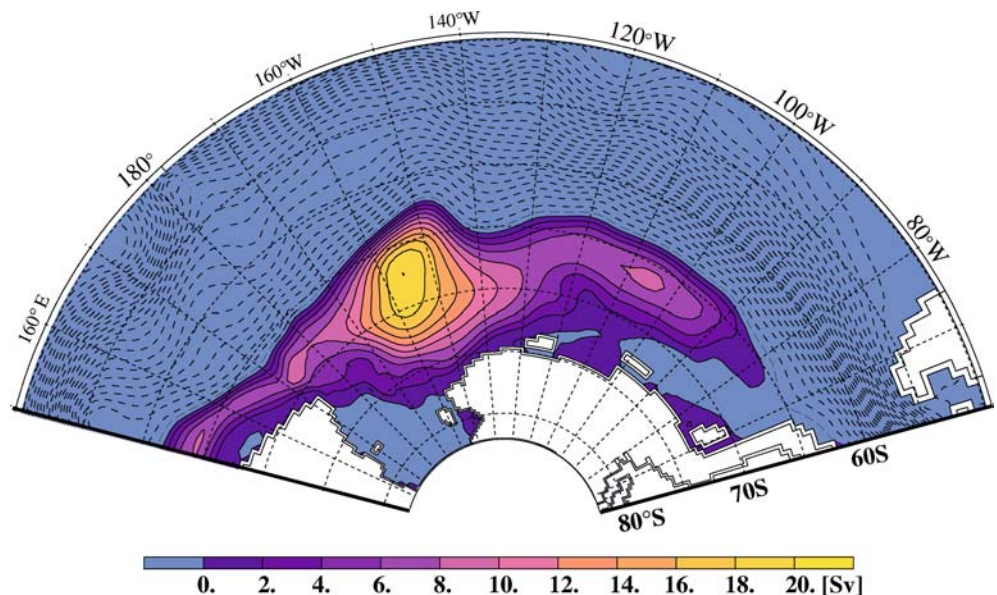
the Antarctic Peninsula would have to be regarded as the gyre's eastern boundary in agreement with inferences from observations by Locarnini (1994).

Simulated maximum gyre transport is ~20 Sv, which is much larger than the volume transport derived from CTD sections. Gouretski (1999) estimated a geostrophic volume transport of 8.5 Sv along 150°W; Locarnini (1994) calculated 5–9 Sv along 170°W. However, neither of these sections cuts through the centre of the main gyre cell shown by the model at 154°W, 67.5°S, a location which agrees with that suggested by Gouretski (1999). In both cases, geostrophic transports have been computed assuming a level of no motion at the bottom or the deepest CTD point. For the Weddell Sea it has been shown that the assumption of a level of no motion is not justified (Gordon et al. 1981; Fahrbach et al. 1991). Total transports can exceed the transport relative to an arbitrary level of no motion by a factor of four and more (Klatt et al. 2005). The difference is due to the fact that the thermal wind equation generally fails to incorporate the velocity shear between the deepest CTD data point and the sea bed, and that thermohaline analysis does not include currents in the boundary layers (where the geostrophic assumption is not valid). Together, this indicates that transports inferred from CTD sections in the Ross Sea tend to underestimate the total transport significantly.

4 Variability of Ross Sea shelf water properties

### 4.1 Time series of temperature and salinity

To investigate the typical salinity and potential temperature variability of the HSSW, a point was chosen north of Ross Island as shown in Fig. 3a. It is located in the centre of the HSSW dome seen in modelled and observed summer salinity sections (Fig. 3b, and Jacobs

and Giulivi 1998) and is hence representative of HSSW characteristics. Choosing a single point prevents the inclusion of spatial averaging artefacts in the time series. The upper water column is subject to a large signal of short-term variability in both salinity and potential temperature, which might obscure longer-term changes. Thus, the monthly mean modelled salinities and potential temperatures were calculated for depths below 300 m for the years 1958–2001. The choice of position north of Ross Island also gives the opportunity of comparison to observations (Jacobs et al. 2002) and model evaluation.

Both time series show an interannual variability with a distinctly larger magnitude than that of the seasonal cycle (Fig. 4). Salinities are within the range commonly associated with HSSW in the Ross Sea and potential temperatures are slightly above the surface freezing point, except for a ~ 0.07°C rise in the 1990s. A Fourier analysis identifies shorter-term variations with characteristic periods of 5 years and 9 years at the 95% significance level. These are superimposed on what appears to be decadal variability.

4.2 Comparison to observations

A freshening of the HSSW in the southwestern Ross Sea since the 1960s has been reported from observations by Jacobs et al. (2002). Their data indicate a decrease in the HSSW salinity of ~0.06 psu at 700 m and ~0.03 psu at 200 m depth between the periods 1963–1978 and 1982–1997. They report a further decrease of approximately equal magnitude for a station taken in February 2000. Naturally, the observational data base is sparse with averages based on five stations between 1963 and 1978 and six between 1982 and 1997 and intervals varying between 11 months and 10 years (Fig. 4). All stations were taken between December and February at a posi-
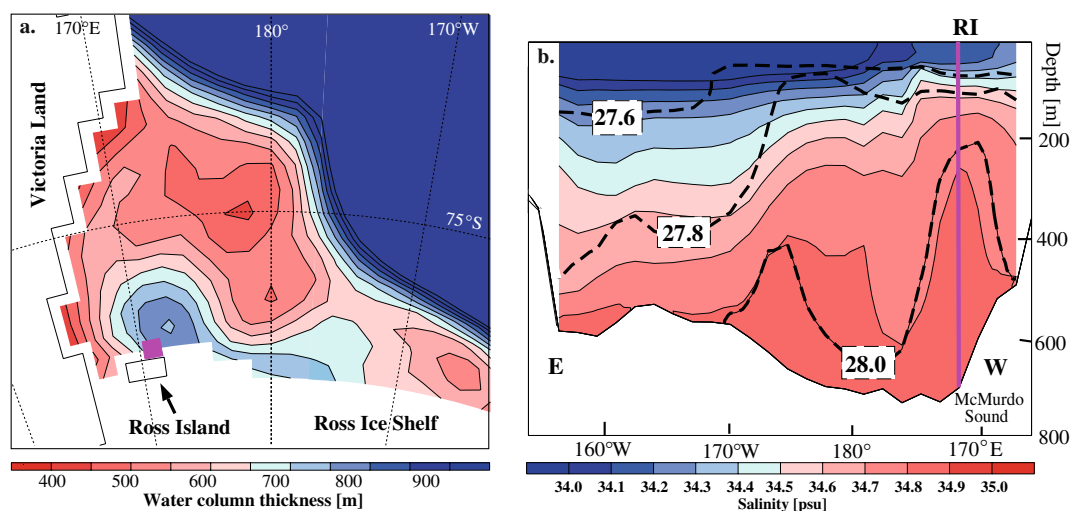
Fig. 3 a Map of model water column thickness for the Ross Sea continental shelf. The position 171.0°E, 77.2°S is marked by the *magenta square*. **b** Modelled section along the Ross Ice Shelf edge, facing south, for salinity (*colour coded*) and density (*thick, dashed contour lines*). The position of the temperature and salinity time series is marked by the magenta line. *RI* Ross Island
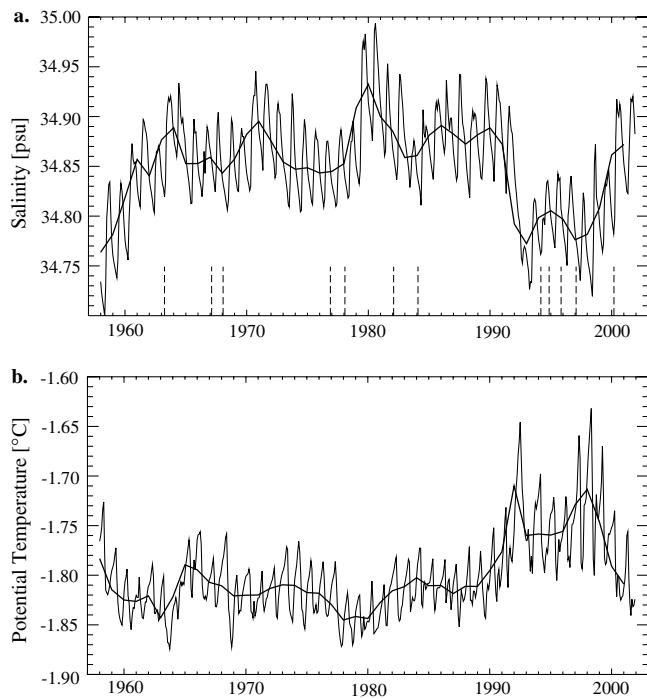
Fig. 4 Simulated monthly (*thin lines*) and annual (*bold lines*) means of **a** mean HSSW salinity below 300 m northeast of Ross Island (171.0°E, 77.2°S as marked in Fig. 3), **b** mean potential temperature for the same position. *Dashed vertical lines* along the time axis in the upper panel indicate the observation times used by Jacobs et al. (2002). Observation times taken from Jacobs and Giulivi (1998) and Jacobs et al. (2002)

tion off the northeastern coast of Ross Island (cf. Fig. 3) with a bottom depth of 900 m.

To compare model results and observations, model results were sampled at 171.0°E, 77.2°S for those months in which the station data were taken. As described above, the point chosen is representative of HSSW conditions in the model and closest to the station locations, being the easterly point north of Ross Island. The model bottom depth is only ∼700 m due to the smoothing of the bottom topography. The data were averaged over the same time periods as in Jacobs et al. (2002), i.e. 1963–1978 and 1982–1997.

The resulting model salinity profiles (Fig. 5) show the same monotonic decrease of HSSW salinities over the 40-year period as observed. Salinities of the 1963–1978 profile are very close to those observed. The salinity decrease towards 1982–1997 is ∼0.04 psu at both 200 m and 700 m, while between 1982–1997 and 2000 a smaller decrease of ∼0.025 psu is seen. Although the model underestimates the magnitudes of variability, the observed decrease of HSSW salinities is reproduced if model data are sampled at the times for which observations are available.

So, following the sampling and averaging intervals of Jacobs et al. (2002), both model and observations suggest a negative trend in salinity for the entire period of observation (1963–2000). However, this feature cannot

be found in the model time series (Fig. 4b). The sampling frequency of the observations obviously is highly irregular and might thus produce aliasing artefacts. The model data were therefore resampled at a regular interval of 5 years for February profiles of potential temperature and salinity, shown in Fig. 6. February profiles were chosen, because end of summer conditions represent the effect of a full seasonal cycle of salinity increase due to brine release and freshening due to summer melting.

The salinity profiles sampled at a 5-year interval reflect the behaviour of the salinity time series shown in Fig. 4. Variability at a period of ∼10 years, i.e. just resolved by the 5-year sampling interval, overlies a longer signal that extends over the whole 44-year (1958–2001) period analysed. While model salinities in the 1990s are indeed lower than those in the preceeding decades, they are not the result of a steady decrease as suggested by Jacobs et al. (2002). The fact that model results show the same behaviour when sampled equivalently to the observations suggests that the strong negative trend described by Jacobs et al. (2002) can be attributed to aliasing as a result of irregular sampling.

As mentioned previously, the Ross Sea continental shelf is one of the most frequently sampled locations in the Antarctic marginal seas. However, it appears that even this extensive data set is insufficient to resolve dense water variability.

Jacobs et al. (2002) comment on potential temperatures being constant throughout the entire period covered by observations and close to the surface freezing point over the entire water column below 200 m. Model potential temperatures are warmer and display more variability with a warm near-surface anomaly apparent in the year 2000 profile (Fig. 5). A possible reason for this is given in Sect. 6.

4.3 Zonal salinity gradient

From both observations (Pillsbury and Jacobs 1985) and model results (Assmann et al. 2003) it has been inferred that the circulation on the Ross Sea continental shelf is predominantly thermohaline driven. Assmann et al. (2003) draw this conclusion on the basis of the seasonal variation of the maximum transport of the anticyclonic circulation cell covering the western shelf and ice shelf cavity in the model and the change in salinity gradient between high and low salinity shelf waters in the western and eastern Ross Sea.

To obtain a quantitative measure of the salinity gradient we compute the difference between the HSSW salinity north of Ross Island and the LSSW salinity below 300 m at the point 171.0°W, 77.8°S for the years 1958–2001. Interannual variability of the resulting gradient is compared to that of the maximum transport of the anticyclonic circulation cell on the Ross Sea continental shelf (Fig. 7). A good correlation ($r = 0.68$), significant at the 95% confidence level, confirms the strong influence of the

Fig. 5 Simulated potential temperature (*left*) and salinity (*right*) profiles below 200 m north of Ross Island averaged following the time slices used by Jacobs et al. (2002). The 1963–1978 profile is an average of five monthly means (February 1963, January 1967, January 1968, December 1976, January 1978), whereas the 1982-1997 profile is an average of six monthly means (January 1982, January 1984, February 1994, December 1994, December 1995, January 1997). Also shown are February 2000 profiles
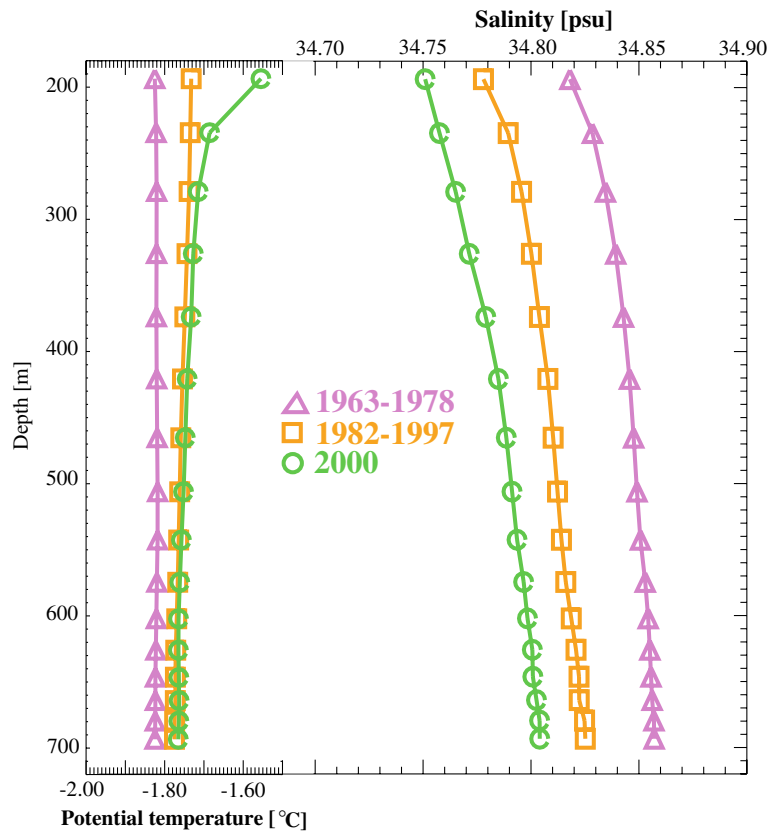
thermohaline structure on the circulation on the Ross Sea continental shelf including the ice shelf cavity.

Noteworthy is also that the salinity difference beween the western and eastern Ross Sea continental shelf remains positive throughout the time period analysed in agreement with observations (Jacobs and Giulivi 1998). In contrast to the shift in the location of the density maximum and the associated change in circulation pattern identified by Timmermann et al. (2002b) on the southern Weddell Sea continental shelf, the circulation pattern and density distribution on the Ross Sea continental shelf do not change their basic shape, but only vary in strength.

## 5 Local atmospheric variability and its effect

5.1 Time scales and sources of variability

Variability of the atmospheric boundary conditions is an important source of interannual variability of water masses in the model and the only external source. Since circulation and water mass distribution at the northern model boundary at 50°S are temporally invariant, signals from lower latitudes can only enter the system through the atmospheric forcing data and not through the ocean. Origins of the interannual dense water variability on the Ross Sea continental shelf thus might either lie in the local atmospheric variability transmitted to the ocean mainly through fresh water fluxes from sea

ice and net precipitation or in circulation changes due to local wind variability. Another possible source is the advection of anomalies in sea ice or ocean which were induced upstream, i.e. in a remote source region, onto the continental shelf.

To determine which atmospheric property is responsible for which part of the variability, the results of two sensitivity experiments are compared to the reference simulation with full atmospheric variability. In the first (NO_T_VAR), a synthetic data set for the 2-m air temperature is used instead of the daily NCEP reanalysis fields from 1948–2001. In the second (NO_UV_VAR), both components of the 10-m winds are replaced by a synthetic data set. These synthetic data sets were computed from the NCEP reanalysis data by calculating a mean annual cycle of the years 1978–1996 and smoothing it with a 30-day running mean. To reinstate short-term variability, the difference between the smoothed and unsmoothed data of 1985 was computed and added to the smoothed 1978–1996 data set. This synthetic data set is perpetually repeated each year for the relevant variable.

Wind variability appears to be the source of the shorter term variations and to generally be the dominant influence on the interannual variability of Ross Sea dense water. The time series of the reference and NO_T_VAR experiments match each other closely while those for NO_UV_VAR are smoother with a larger seasonal cycle (Fig. 8). The variability of dense water volume and HSSW salinity in the standard run
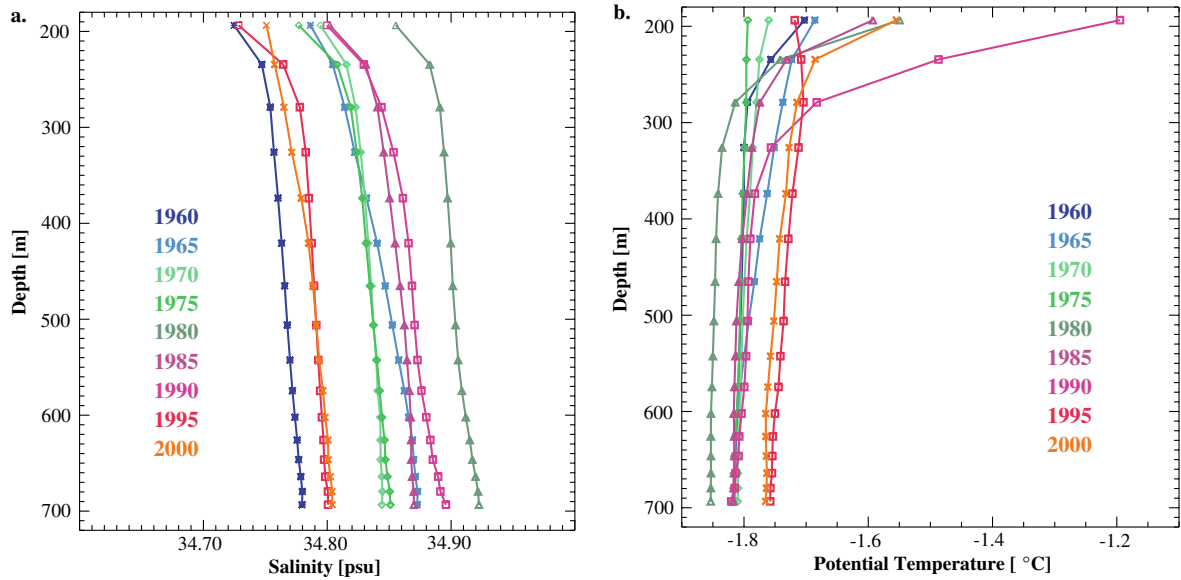
Fig. 6 Simulated **a** salinity and **b** potential temperature profiles below 200 m north of Ross Island. February profiles are shown at 5-year intervals for the years *colour-coded*

appears to be a superposition of a short-term signal induced by wind variability onto a smoother signal with variability on the order of several decades induced by air temperature variability. While a Fourier analysis of the time series reveals that the wind induced variability is periodic at 5–6 and 9 years, there is no obvious periodicity in the air temperature induced signal. If periodic, the model results suggest a period of ~40 years, which is close to the 44-year time period analysed, so this has to remain speculation.

Summer events of strong easterlies in the standard and NO_T_VAR runs prevent the sea ice from being driven northeastward and from melting north of the continental shelf. Instead, fresh melt water is added to the water column in the southwestern Ross Sea lowering HSSW salinities the following winter. Since events of strong northeasterly summer winds do not exist in the synthetic data sets of the NO_UV_VAR experiment, HSSW salinities are around 0.15 psu higher than in the other two sensitivity experiments.
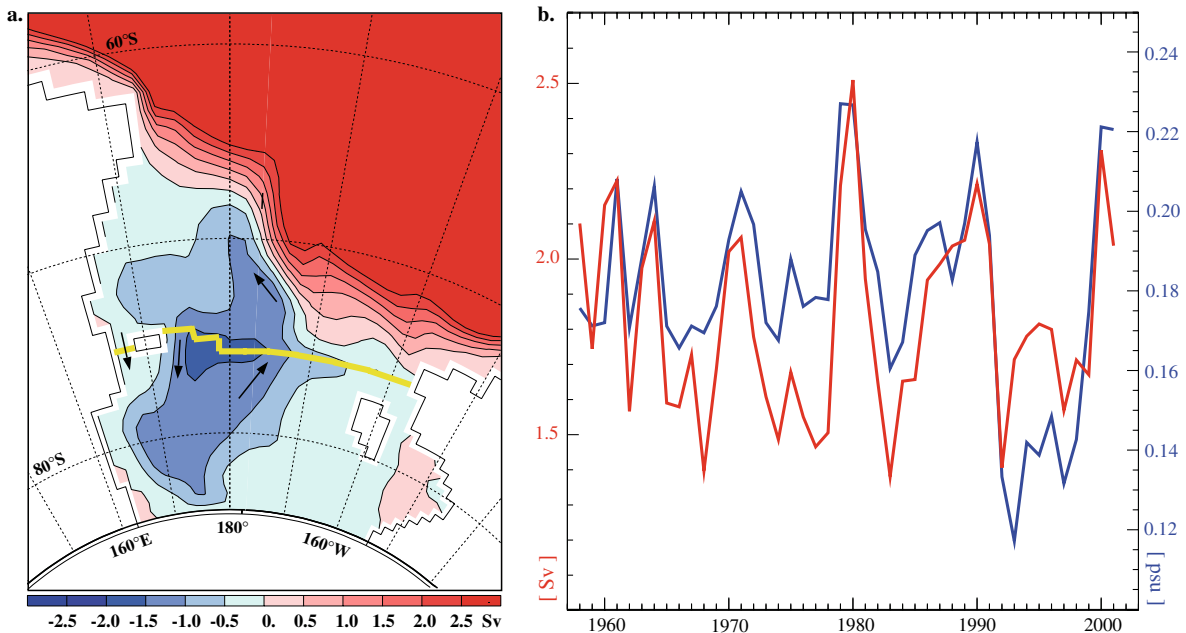
Fig. 7 a Long-term mean simulated vertically integrated transport (stream function) on the Ross Sea continental shelf and in the Ross Ice Shelf cavity. **b** Detrended model time series of annual means of the maximum transport of the anticyclonic circulation cell on the Ross Sea continental shelf (*red, left scale*) and the salinity difference between High and Low Salinity Shelf Water (*blue, right scale*)

Fig. 8 For the reference simulation (*black*) and two sensitivity experiments (*colour coded*): monthly (*thin lines*) and annual (*thick lines*) means of **a** mean HSSW salinity below 300 m northeast of Ross Island (171.0°E, 77.2°S as marked in Fig. 3), **b** mean potential temperature for the same position
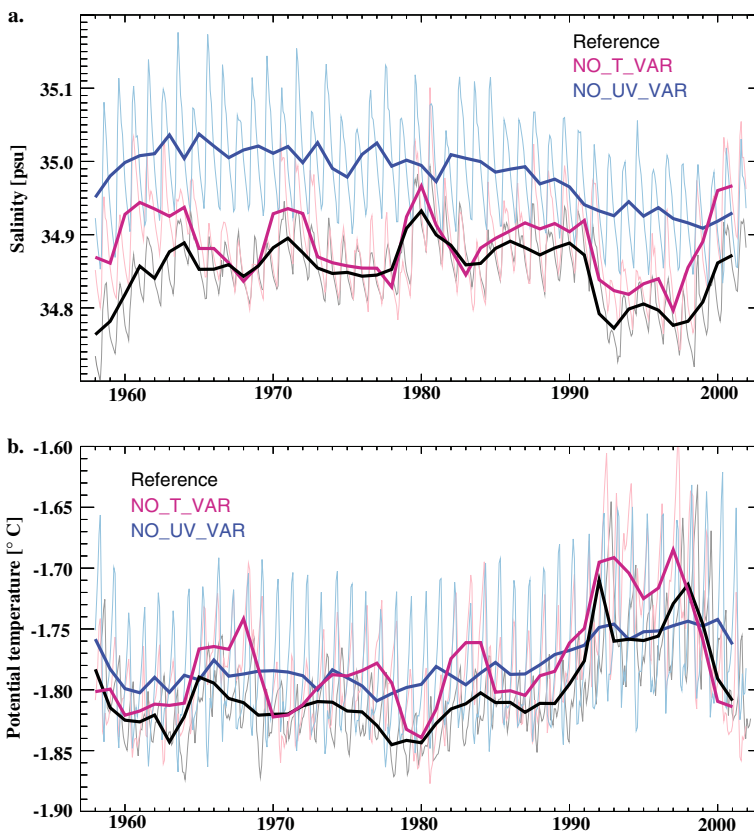
5.2 Fresh-water fluxes

Surface fresh-water fluxes on the Ross Sea continental shelf are dominated by sea ice formation and melting and its variability (Fig. 9). With a mean annual value of 27 mSv the fresh water extraction due to sea ice formation represents the largest term in the fresh-water budget. Annual mean fresh-water fluxes due to net precipitation and ice shelf basal melting are much smaller with annual means of 4–6 mSv.

Noteworthy, however, is the strong dependence of ice shelf basal melting on wind variability (Fig. 9c). Model results (Assmann 2003) show that melting at the ice shelf front contributes about 40% to the total basal mass flux of the Ross Ice Shelf cavity with large summer peaks seen in Fig. 9c caused by warm summer surface waters coming in contact with the ice shelf base. In summer, winds can act on the ocean surface unperturbed by sea ice and drive warm surface waters southwestward towards the ice shelf front. Even in the inner cavity, a summer maximum in the basal melt rate appears due to a wind-driven inflow (Assmann 2003). Since the annual mean basal melt rate is dominated by this summer peak, the lack of wind variability in NO_UV_VAR explains the nearly constant annual mean basal melt rate in this experiment. Thus, these sensitivity studies prove the importance of wind fluctuations for determining the variability of ice shelf basal melting.

However, for both ice shelf basal melting and net precipitation rates, the range of variation of around 3 mSv is small enough to make them act as a near constant source of fresh water. Thus, variability of fresh-water fluxes is mainly imposed by the sea ice. The analysis of the local fresh water and atmospheric variability on the Ross Sea continental shelf will hence concentrate on the sea ice fresh-water flux.

The southwestern Ross Sea is enclosed by boundaries of land and ice shelf to the south and west. Thus, southwesterly winds lead to a divergent ice pack and strong sea ice formation, while winds with a northerly or easterly component have the opposite effect. For the reference simulation, there is a good negative correlation ($r = -0.67$) between the annual mean southwesterly wind component (Fig. 10a) and the sea ice fresh-water flux; strong southwesterly winds cause a large negative fresh water flux/strong brine release. For monthly means, correlations significant at the 95%-level ($r \geq -0.6$) appear between April and October with the fresh-water flux lagging the winds by 1 month. There is no significant correlation of fresh-water flux with the southwesterly wind component between November and March when air and ocean surface temperatures approach the freezing point. In November, December, and March, however, a positive correlation with air temperatures is found to be significant at the 95% level. The onset of melting and freezing during this period is determined by air temperatures approaching the freezing point and warming or cooling the ocean surface.

However, there is no significant correlation between the time series of annual mean air temperature (Fig. 10b)
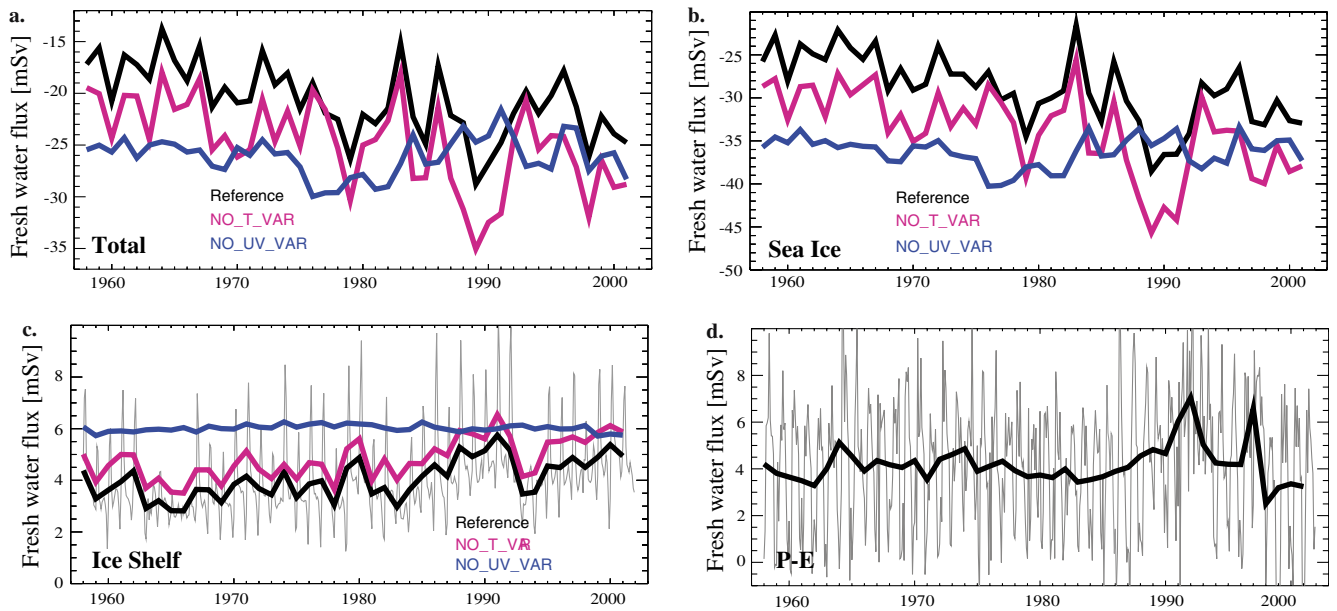
Fig. 9 Time series of modelled fresh-water fluxes on the Ross Sea continental shelf (bottom depth ≤ 1000 m). **a** Total fresh-water flux. **b** Fresh-water flux due to sea ice production and melting. **c** Basal mass flux in the Ross Ice Shelf cavity, annual means (*thick lines*) and monthly means for the reference simulation (*thin black line*). **d** NCEP net precipitation, annual (*thick line*) and monthly means (*thin line*)

and sea ice fresh-water flux. Instead, as discussed above, wind variability appears to be the dominant influence on the interannual variability of the fresh-water flux due to sea ice. In NO_T_VAR, i.e. without temperature variability, the correlation between the annual mean southwesterly wind component and sea ice fresh-water flux rises to $r = -0.81$. The strong dependence of the sea ice fresh-water flux on the winds confirms that the Ross Sea Polynya is predominantly a latent heat polynya as suggested by Zwally et al. (1985). Only in NO_UV_VAR does the air temperature variability have a significant influence on the sea ice fresh-water flux, again mainly in spring and autumn and not reflecting the increase in the variability of NCEP air temperatures after 1978.

5.3 Effect on HSSW

Surprisingly, there is no significant correlation between the sea ice fresh-water fluxes and HSSW salinities in any

of the three experiments (Figs. 8a, 9b). Since changes in the sea ice fresh-water flux are small (∼6 mSv) in NO_UV_VAR, this result might be expected in this case. However, wind induced changes in the other two experiments represent a considerable proportion of the annual mean surface fresh-water flux. Strong peaks in brine input around 1980 and 1990, and minima in the mid-1980s and 1990s correspond to maxima and minima in HSSW salinity, but the relative amplitude of the fresh-water extrema is not reflected in the salinities.

The annual cycle of sea ice fresh-water flux has an amplitude of ∼150 mSv (Assmann et al. 2003) and translates to a seasonal salinity change of around 1 psu at the model sea surface. Fig. 8a shows that this seasonal cycle is damped to around 0.1 psu below 300 m. Year-round observations in McMurdo Sound reveal a similar attenuation of the seasonal salinity signal within the water column from 0.8 psu at the surface to 0.2 psu below 300 m (Tressler and Ommundsen 1962).
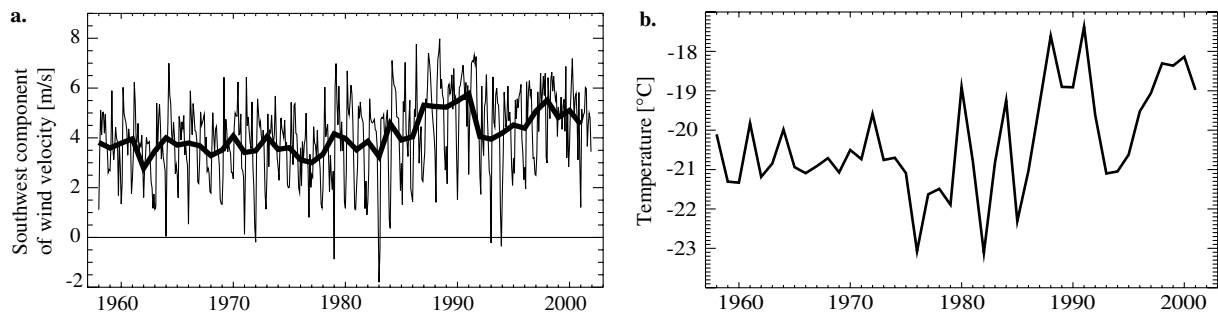
Fig. 10 Time series of NCEP reanalysis data in the southwestern Ross Sea. **a** Monthly (*thin line*) and annual (*thick line*) means of the southwesterly wind component. **b** Annual mean air temperatures

The maximum sea ice freezing rate occurs in April when the continental shelf is mostly ice-free or ice concentrations are low. Thus the wind-driven surface currents are still strong (4–5 cm s^{-1}), advecting much of the peak salinity signal out of the area where HSSW is formed, before convection reaches its full strength. Hence, the interannual variability of the fresh-water flux is already attenuated in the surface layer. Since even the large seasonal cycle of sea ice induced salinity variation is reduced significantly towards greater depths, the much smaller interannual variations are altered almost beyond detection.

In agreement with Jacobs et al. (2002) it can be concluded that the interannual variability of local fresh-water input does not trigger the dense water variability on the Ross continental shelf, but that brine release in the Ross Sea polynya only raises the salinity to the level associated with HSSW within the seasonal cycle. Instead, the interannual variability seems to have its origin in a remote source and is carried onto the continental shelf with the inflowing waters.

## 6 Inflow variability to the continental shelf

6.1 Analysis strategy

Assmann et al. (2003) suggested that fresh-water import with the coastal current onto the Ross Sea continental shelf balances the 18 mSv of net fresh-water extraction calculated in a budget of the local fresh-water sources and sinks. Consequently, the shelf inflow appears to be a strong candidate to carry signals of interannual salinity and potential temperature variability onto the Ross Sea continental shelf.

Following Jacobs and Comiso (1989) the continental shelf break is defined as the 1,000 m isobath for this study. The variability of water flowing onto the shelf across this line is taken to represent the inflow characteristics and variability. For analysis, the continental shelf break was split into a western part from Cape Adare to Pennell Bank, a central part that runs almost meridionally along the eastern side of Pennell Bank, and an eastern part that extends near-zonally to Cape Colbeck (Fig. 11).

Model results suggest that inflows near the surface are located in the eastern and central parts of the shelf break, while near the bottom flow onto the continental shelf only occurs in the central part of the Ross Sea (Assmann et al. 2003). To capture the vertical variation within the water column, time series of the mean inflow salinity and potential temperature are calculated for 100 m bins for the eastern and central sections of the continental shelf break.

6.2 Salinity

Similar to the attenuation of surface-induced variability (see Sect. 3), the amplitude of the salinity variability in
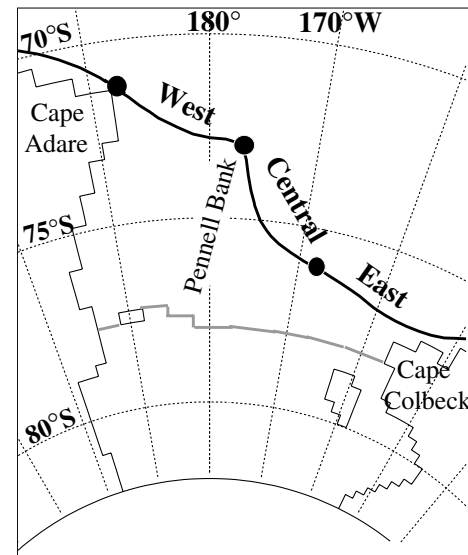

Fig. 11 Map of the Ross Sea with the 1,000 m isobath marked as represented by the model. *Marked by dots* are the boundaries of the western, central and eastern sections. The *grey line* represents the ice shelf front

the continental shelf inflow is attenuated towards greater depth in all three experiments (Fig. 12). The inflow salinity time series in the reference simulation and the sensitivity experiments have similar characteristics in their variability as their HSSW counterparts with salinities below 600 m being nearly homogeneous. Those including wind variability show shorter, periodic signals, while variability in the NO_UV_VAR experiment (not shown) again is smoother. Unlike on the continental shelf, the absence of wind variability does not induce an increase in salinity of the inflowing water. This reflects the presence of the large volume of CDW with near-constant salinity which dominates the inflow at depth.

Modelled salinities in the top 200 m of the water column show a negative trend that matches that identified by Jacobs et al. (2002) in observed salinities between 25 m and 130 m closely in both magnitude and absolute values.

To quantify the connection between shelf inflow and dense water properties and to identify the depth at which salinity and potential temperature signals are carried onto the continental shelf, a correlation analysis was performed for the eastern and central shelf break segments. Its results are summarised in Table 1.

Significant correlations between the inflow and HSSW salinities are found within the top 300 m of both the eastern and central segments of the shelf break in agreement with the main inflow locations at this depth. Stronger correlations and shorter lags for the central segment reflect the westward advection of the salinity signal towards the region of HSSW formation. In the previous section the strong attenuation of the seasonal and interannual surface salinity signals due to sea ice formation was mentioned. Much of this attenuation
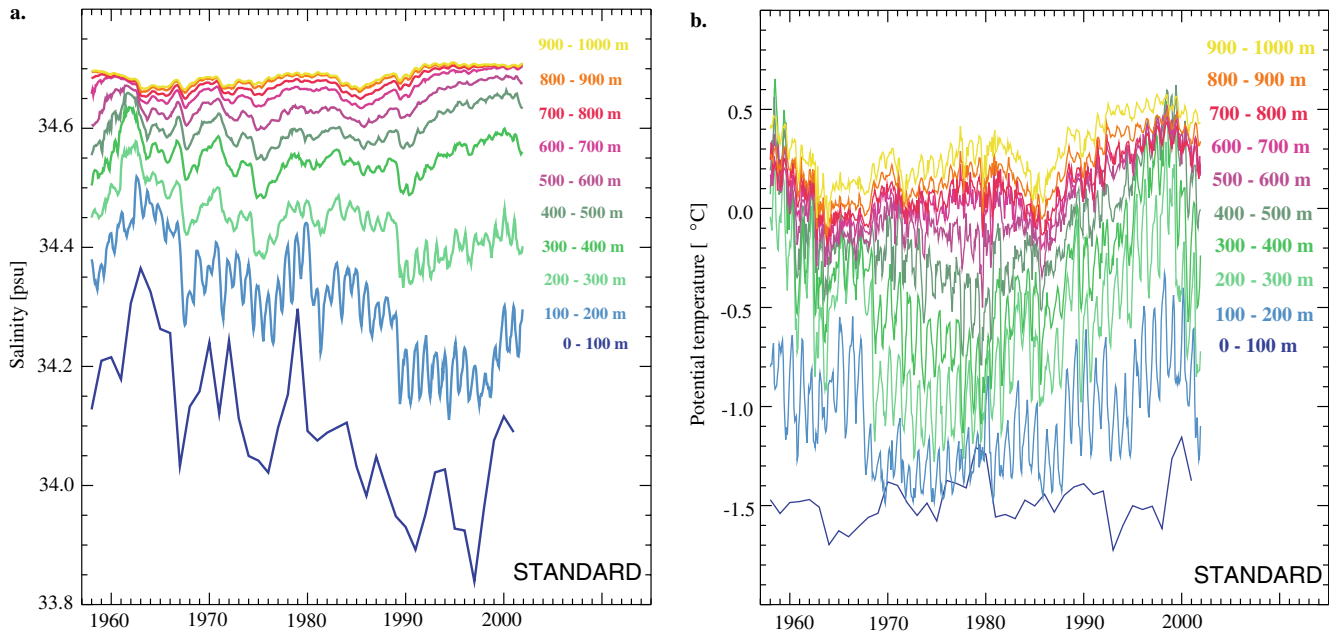
Fig. 12 Simulated characteristics of the Ross Sea continental shelf inflow: time series of **a** salinity for the eastern section and **b** potential temperature for the central section. *Depth is colour coded.* For the interval 0–100 m annual rather than monthly means are shown

occurs in the top 50 m of the water column where wind influence and the associated advection are strongest. For the top 100 m, correlations between inflow and HSSW salinities are strongest in winter when ice cover reduces the wind influence on the surface currents and exchange between the top 100 m and the HSSW is strongest due to deep convection. Below 100 m the thermohaline-driven and topography guided circulation pattern described in Assmann et al. (2003) gains importance and the correlation loses its seasonal dependence enabling the salinity signal to be transmitted to the HSSW without major attenuation.

Table 1 Table of correlation coefficients between time series of salinity and potential temperature at the continental shelf break and in the HSSW

	Salinity		Potential temperature	
	East	Centre	East	Centre
100		0.70(1)		
200	0.56(2)	0.74(1)	0.55(0)	0.61(0)
300	0.55(2)		0.70(0)	0.64(0)
400			0.72(0)	0.73(0)
500			0.72(0)	0.79(0)
600			0.70(0)	0.79(0)
700			0.65(0)	0.75(0)
800			0.64(0)	0.72(0)
900			0.64(0)	0.70(0)
			0.62(0)	0.69(0)

The number in brackets are lags in years, with positive lags denoting HSSW time series lagging behind those at the continental shelf break. Only correlation coefficients significant at the 95% level are given
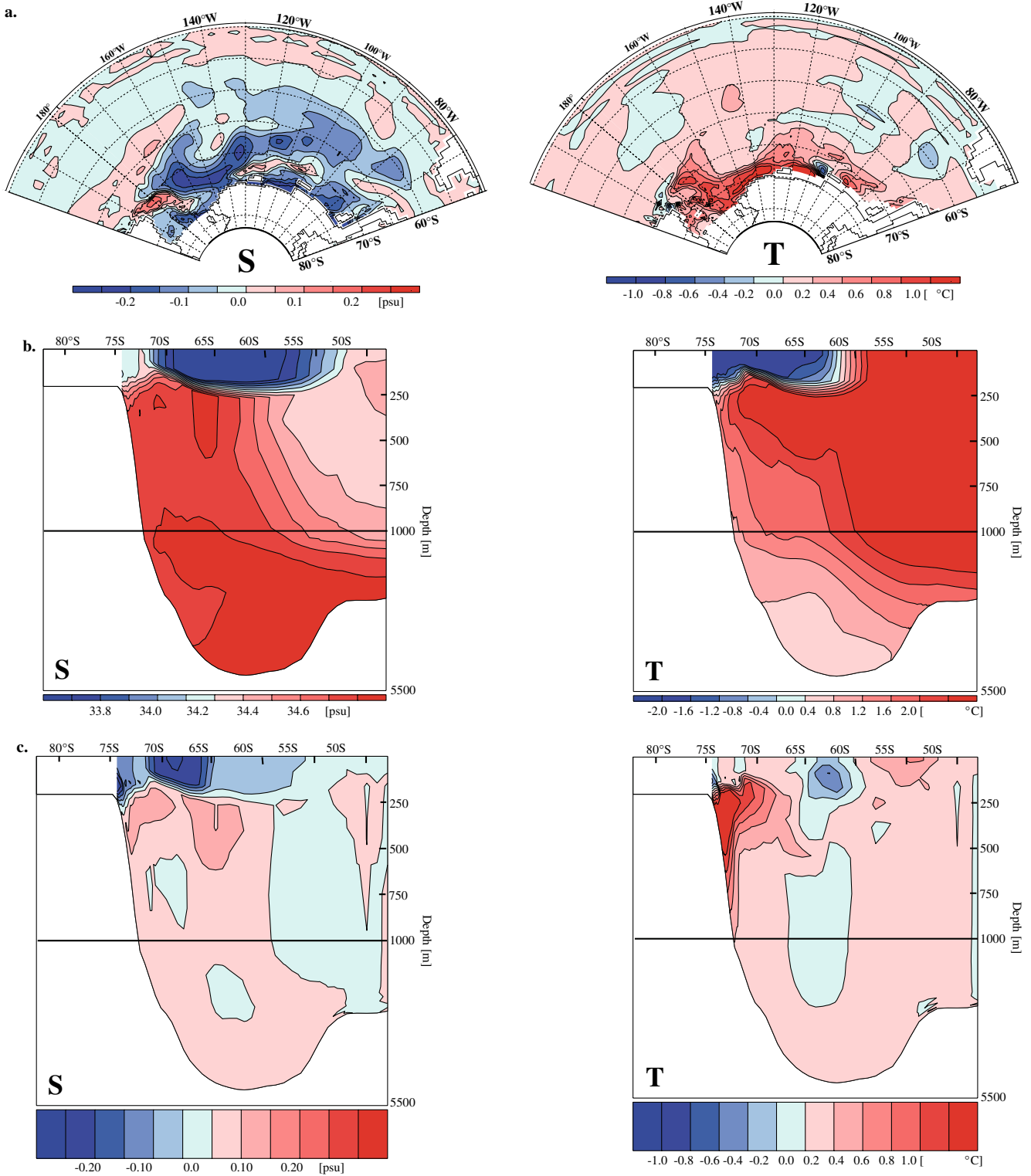
6.3 Temperature

Unlike the salinity variability, the potential temperature time series show variability at large amplitudes all through the water column to the bottom. Those for the standard run (Fig. 12b) and the NO_T_VAR experiment (not shown) feature the large warming peak in the 1990s familiar from the HSSW potential temperature series (Fig. 8b). The signal of potential temperature variability is strongest between 300 m and 700 m within the core of the coastal current—in contrast to the salinity signal which is transmitted above this depth (Table 1). As the inflow to the continental shelf is located in the central shelf break segment for this depth range, correlations between HSSW potential temperature and the inflow on the eastern segment are weaker.

In contrast to the observations (Jacobs et al. 2002), model results show near-bottom potential temperature variations of about 0.1°C (Fig. 6). We attribute this discrepancy to the smoothing of bottom topography (Fig. 1) due the relatively coarse model resolution and the necessities of model numerics. This leads to a narrower continental shelf with a less abrupt shelf break and smoother topographic features. As a consequence, MCDW carrying potential temperature variability can enter the continental shelf further and in greater quantites than in reality, which in turn leads to the presence of the potential temperature signal in the HSSW as well as to higher modelled HSSW temperatures than observed.

6.4 Implications

We have shown that variations of salinity and potential temperature enter the continental shelf at different

Fig. 13 For the reference experiment, monthly mean for September 1997. **a** *Left*: Salinity anomaly at 150 m. *Right*: Potential temperature anomaly at 400 m. **b** Meridional salinity (*left*) and potential temperature (*right*) section along 115°W, i.e. in the central Amundsen Sea. **c** Salinity (*left*) and potential temperature (*right*) anomalies for the same sections. The top 1,000 m of the water column are stretched for better visibility in **b** and **c**

depths, even though both signals appear to originate to the east of the Ross Sea. The inflow signal can be identified clearly in the HSSW characteristics. The in-

terannual variability of dense water characteristics can thus be attributed to a source external to the Ross Sea continental shelf, with local sea ice formation only

leading to a salinity enhancement during the seasonal cycle. A strong anticorrelation of HSSW salinity and potential temperature time series ($r = -0.71$ for the standard run) suggests that both have either a common origin or the one is induced by the other, though the signals then propagate at different depths.

7 Origin in the Amundsen and Bellinghausen seas and propagation

7.1 Anomaly patterns

To investigate the propagation paths and the area of origin of the salinity and temperature anomalies that enter the Ross Sea continental shelf, two core depths are chosen which were found to carry the characteristic signals responsible for the HSSW variability (cf. Sects. 5, 6). These are 150 m for the salinity anomaly and 400 m for the potential temperature anomaly. September 1997 was chosen for demonstration purposes, since this month represents winter conditions at the end of the warm and fresh HSSW anomaly.

The salinity and potential temperature anomalies show the anticorrelation familiar from the HSSW signals. Both signals are spread throughout the Amundsen and Bellingshausen Seas (Fig. 13a). Their amplitudes are largest in the Amundsen Sea close to the coast and are attenuated as they enter the Ross Sea continental shelf.
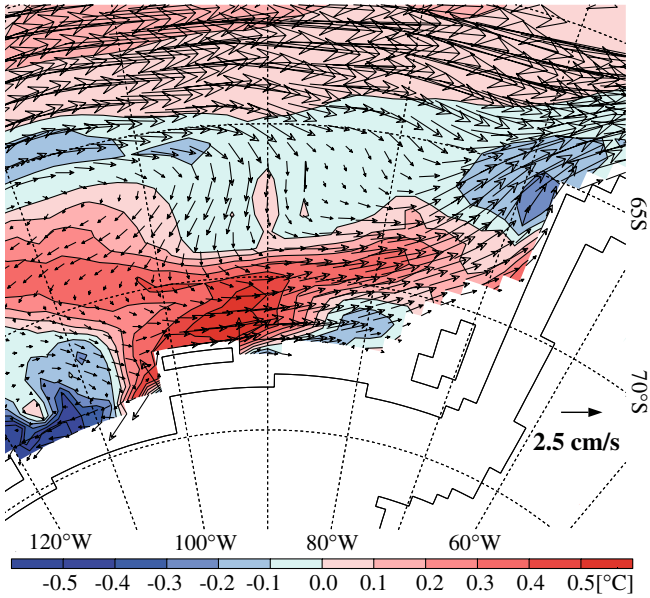
On a meridional section at 115°W, i.e. through the centre of the Amundsen Sea, salinity anomalies with amplitudes ≥0.1 psu are confined to the top 200 m in agreement with results from the previous section at the Ross continental shelf break (Fig. 13c, left panel). This layer is subject to a large seasonal cycle and strongly feels the effect of sea ice formation and melting, suggesting that the salinity anomalies are connected to surface fresh water input due to sea ice.

The core of the potential temperature anomalies is located in the southern extension of the CDW which reaches and enters the continental shelf in the Amundsen Sea (Fig. 13c, right panel). Amplitudes are large, up to 1.5°C, and reflect how closely the warm CDW core approaches the shelf and how much its mixing with colder shelf waters varies. The maximum potential temperature anomaly is found on the continental slope close to the bottom between 200 m and 1,000 m depth. A northward extension reaches 65°S between 200 m and 500 m. CDW salinities at this depth are fairly constant just above 34.7 (Fig. 13b) and the amplitude of anomalies is small (see also Fig. 12). These temperature anomalies appear to be equivalent to a westward travelling bottom potential temperature anomaly within the coastal current proposed by Beckmann and Timmermann (2001) who refer
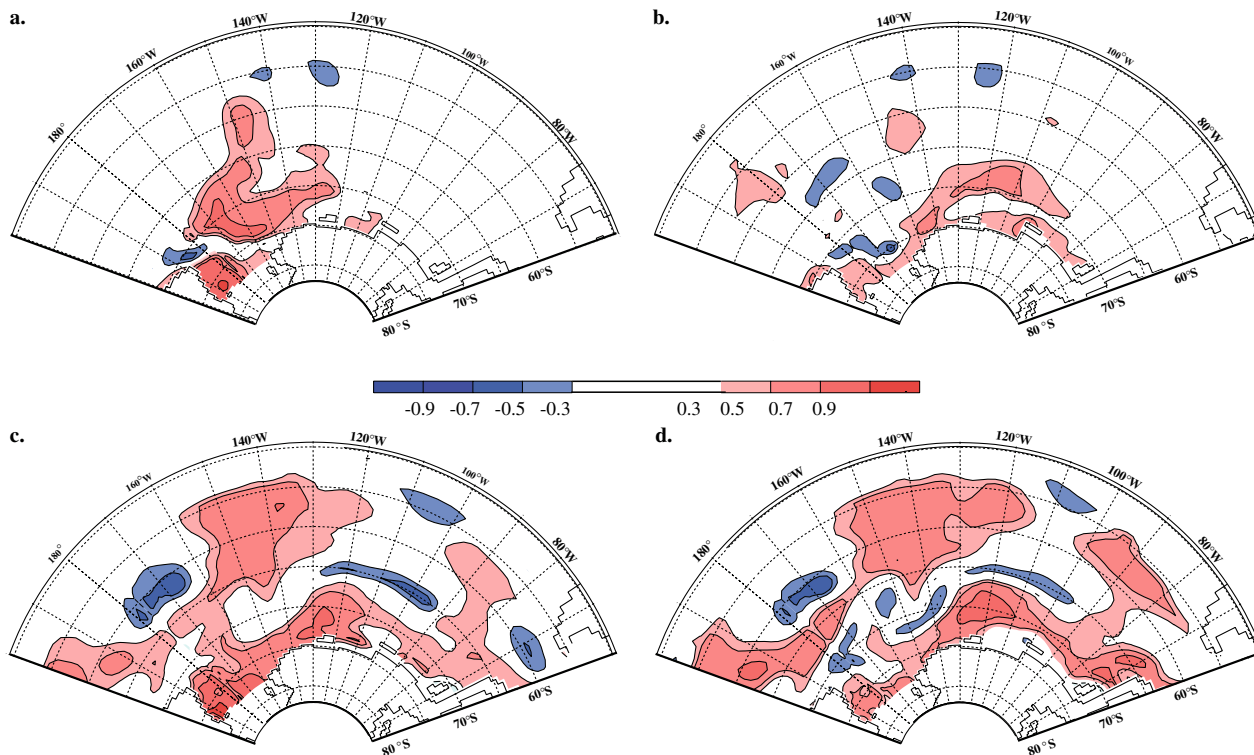
Fig. 14 Cross-correlation maps for simulated annual means of a HSSW salinity onto salinity at 150 m depth, zero lag, b HSSW salinity onto salinity at 150 m depth, 5-year lag, c HSSW potential temperature onto potential temperature at 400 m depth, zero lag, d HSSW potential temperature onto potential temperature at 400 m depth, 5-year lag. Correlation coefficients $|r| > 0.5$ are significant at the 99% significance level

Fig. 15 Simulated potential temperature anomaly (*colour coded*) and current velocities (*vectors*) at 400 m for September 1984 at the start of a warm anomaly in the standard run

signals. Both salinity and potential temperature show a strong positive correlation for zero lag on the southwestern Ross Sea continental shelf where the HSSW formation region is located.

Outside the continental shelf area the salinity and potential temperature signals follow quite different paths. At the eastern end of the Ross Sea continental shelf the salinity signal is split. Besides entering the Ross Sea continental shelf, part of the salinity signal propagates along the continental shelf break (Fig. 14a). With HSSW salinities lagging those at 150 m by 5 years a significant correlation is confined to the coast in Amundsen and Bellingshausen Seas and to a region between 65°S and 70°S in the Amundsen Sea where $r \geq 0.5$ (Fig. 14b). This indicates that the salinity signal is induced in the Amundsen and Bellingshausen Seas and puts a timescale of around 5 years to the propagation of the salinity signal from its origin to the Ross Sea in agreement with estimates from current speeds at this depth.

In contrast to the closely confined salinity signal, the temperature signal (Fig. 14c, d) can be identified in large parts of the basin. For both zero and 5-year lags good correlations are found in the Amundsen Sea. Maximum correlations for salinity and temperature both are located in the southern limb of the Ross Gyre at about 130°W, where the coastal current shifts southward following the topography of the continental slope (cf. Figs. 1, 2). Noteworthy are also large areas of significant correlation around 60°S north of the Bellingshausen and eastern Ross/western Amundsen Seas. Both indicate propagation paths of the signal apart from that onto the Ross Sea continental shelf. As with the salinity signal, the potential temperature signal follows the western branch of the Ross Gyre north. The potential temperaure signal is also carried northward into the ACC and eastward around the Antarctic Peninsula, since the current pattern at 400-m depth is still influenced by that at the surface, and velocities in the Bellingshausen Sea are directed northeastward (Fig. 15). The amplitudes of potential temperature anomalies are small, however, in

to it as the Antarctic circumpolar coastal wave (ACCW). Their analysis also shows a warm anomaly in the Ross Sea in the 1990s in agreement with the results presented here. Rather than being confined to potential temperatures, there appears to be an equivalent in salinity, which, however, propagates closer to the surface.

7.2 Propagation paths

Maps of cross-correlation coefficients of the HSSW salinity time series with salinity at 150 m and of HSSW potential temperatures onto potential temperature at 400 m depth (Fig. 14a, c) shed light on the origin and propagation paths of the HSSW interannual variability

Fig. 16 Crosscorrelation map of simulated salinity at 150 m and simulated potential temperature at 400 m for detrended annual means, zero lag. Correlation coefficients $|r| > 0.5$ are significant at the 99% significance level
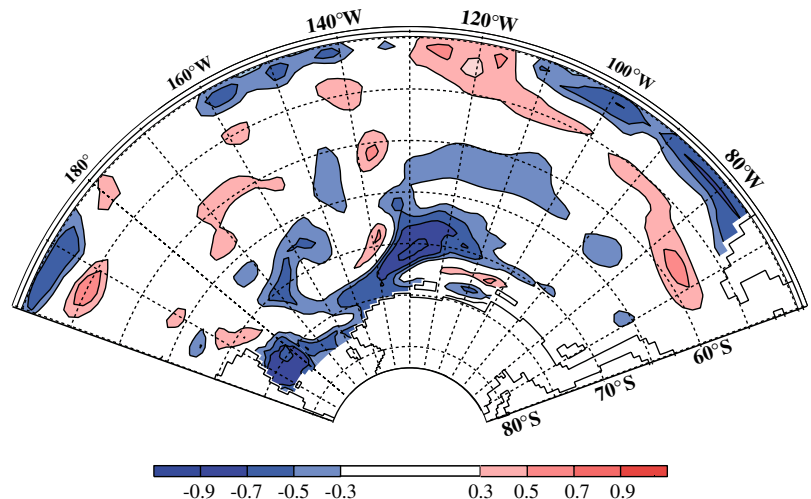
both of these areas due to mixing processes occurring in the fast-flowing ACC regime.

The cross-correlation maps in Fig. 14 also confirm the path salinity and potential temperature anomalies take onto the Ross Sea continental shelf as postulated in Sect. 6. The salinity anomaly propagates close to the coast between 150°W and 170°W to enter the continental shelf at its eastern end. At 400 m and hence well within the influence of the bottom-intensified westward flow of the coastal current the potential temperature signal is advected onto the shelf both in the eastern and central Ross Sea.

The idea that salinity and potential temperature variability are connected despite their propagation at different depths and that the connection is established in the Amundsen Sea is confirmed by a crosscorrelation of salinity anomalies at 150 m and potential temperature anomalies at 400 m. Strong anti-correlations ($|r| > 0.8$) exist in the Amundsen Sea between 67°S and 72°S (Fig. 16). They also trace the propagation path of the salinity signal onto the Ross Sea continental shelf close

to the coast and show the northeastward advection of the signals with the western limb of the Ross Gyre. The correlation breaks down above the continental slope where water with a different salinity signature is advected southeastward.

7.3 Mechanisms of vertical exchange

This section discusses the connection between sub-surface salinities and 400-m potential temperatures in the Amundsen Sea. The region of interest, the Amundsen Sea between 67°S and 72°S and 110°W and 130°W, is located within the marginal sea ice zone, near the winter sea ice edge, where strong interannual anomalies of sea ice concentration and growth rate exist. Convection during the sea ice growth season would hence be a likely candidate for a vertical exchange mechanism between 150 m and 400 m. A negative anomaly in brine release would lead to lower salinities in 150 m depth, a more stable water column, less convection, and hence to
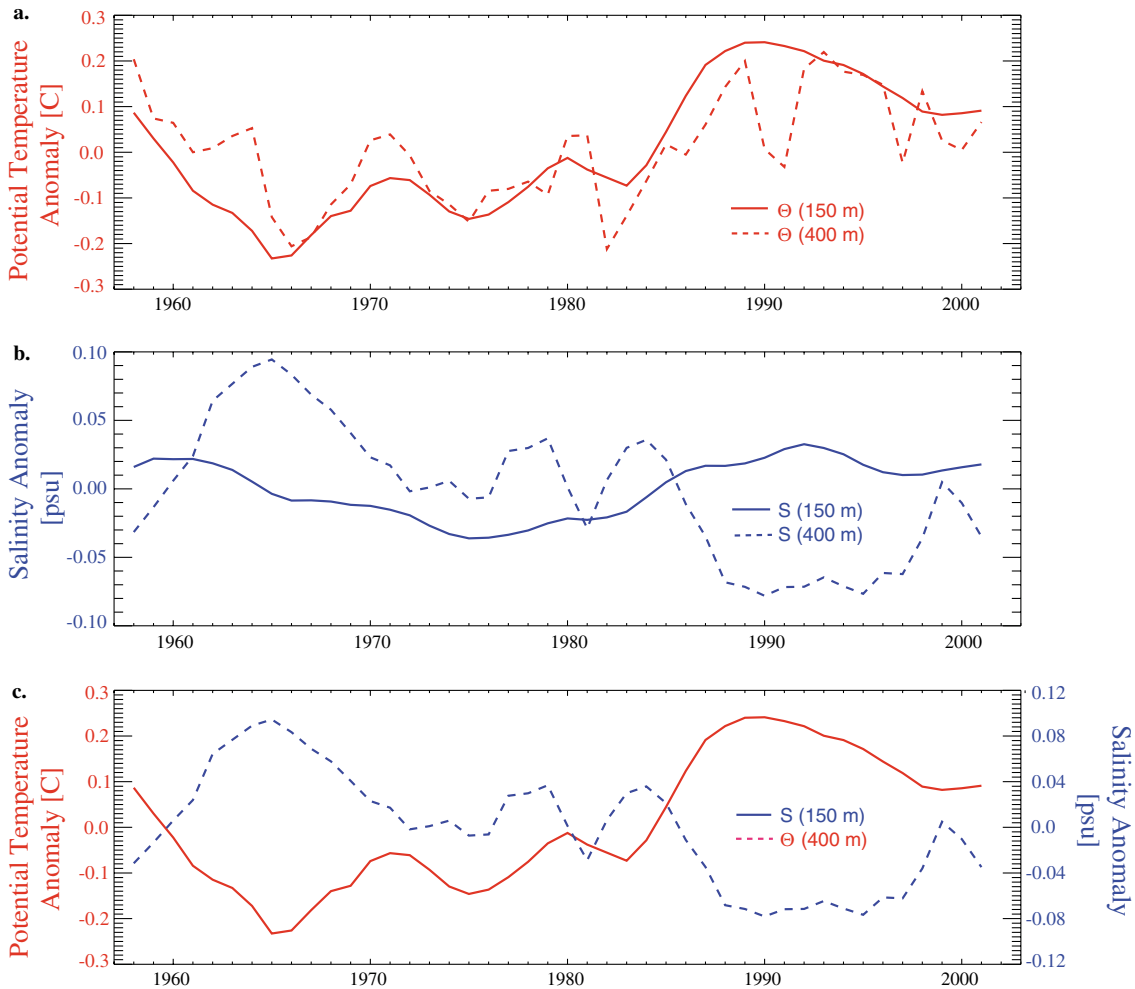
Fig. 17 Detrended time series of simulated annual mean **a** potential temperatures at 150 m and at 400 m, **b** salinity at 150 m and at 400 m, and **a** potential temperatures at 400 m (*left scale*) and salinities at 150 m (*right scale*). Potential temperatures and salinities are averaged over the region 67°S and 72°S and 110°W and 130°W at their respective depths

higher temperatures in 400 m depth, or vice versa. Time series of annual mean temperatures and salinities indicate that potential temperatures at 150 m and 400 m are positively correlated in the region of interest with variability at shorter time periods in the sub-surface waters overlying the longer-term signal of the deep ocean (Fig. 17a). However, salinities at these depths only show a weak negative correlation not significant at the 99% level, i.e. salinities at 400 m do not appear to be affected by sub-surface salinity anomalies (Fig. 17b). If signals of variability were transmitted through vertical mixing, salinities and potential temperatures should show correlations of the same sign, which does not agree with our results. Given in addition that mixed layer depths even in winter do not exceed 200 m in this model region, we conclude that convective mixing is not the dominant process here.

The maximum anticorrelation between salinities at 150 m depth and temperatures at 400 m (Fig. 16) is found around the position 130°W, 70°S, where the southern limb of the Ross Gyre is shifted strongly southward following a southward turn of the continental shelf break (cf. Figs. 1, 2). This area coincides with the transition zone between the easterly winds along the coast and the westerlies further north. Ekman pumping enables the distinctively cyclonic mean wind field in this region to cause local oceanic upwelling. In the 44-year mean, the maximum upwelling velocity is 10 cm/day, but in the monthly means vertical velocities of 30 cm/day are common. The strongest upwelling occurs in winter, when vertical temperature gradients are largest and the vertical velocities are sufficiently large for warm CDW to cross a narrow thermocline of only 30–50 m thickness (Fig. 13b).

Upwelling of warm CDW thus offers a mechanism for signals at 400 m depth to propagate upward towards the surface. The positive correlation between potential temperatures at 150 m and 400 m depth confirms this hypothesis. Salinity anomalies at 400 m depth are small (Fig. 13c); thus, even if upwelling carries these signals into the upper ocean, the larger salinity anomalies induced at the surface will cancel their effect.

The negative correlation between potential temperatures at 400 m depth and sea ice growth rate anomalies (Fig. 18a), and the positive correlation between sea ice growth rate anomalies and sub-surface salinities at 150 m (Fig. 18b) confirm that higher temperatures at 400 m depth cause lower sea ice growth or stronger melting, which in turn creates anomalies of surface and sub-surface salinity. Since mixed layer depth even in winter does not exceed 200 m in the region in question, these salinity anomalies are confined to a sub-surface layer and do not penetrate down to the 400 m level. Note that the mechanism proposed here only acts in the northern Amundsen Sea, in the region of a strongly cyclonic wind field. Near the coast, easterly winds lead to an onshore Ekman transport which results in downwelling at the continental shelf break, thus preventing upward heat flux from the core of the temperature anomaly (Fig. 13c) from affecting the sea ice cover along the coast.

Although the curl of the large-scale wind field seems to be responsible for transmitting signals between the different levels, we do not find a correlation between its anomalies (not shown) and the variability in the 150 m depth level. Thus, although the spatial pattern of wind stress curl is crucial to the interaction between the deep and the subsurface ocean in this region, its interannual variations do not seem to have a big effect on ocean variability.

The physical mechanism that links the potential temperature anomalies at 400 m depth to the sub-surface salinity anomalies, which in the end determines HSSW salinity and potential temperature on the Ross Sea continental shelf, can thus be summarised as follows: Upwelling of CDW in regions with a strongly cyclonic surface wind stress causes an upward heat flux that reaches the surface near the sea ice edge in the Amundsen Sea. This induces anomalies of sea ice fresh water flux which lead to sub-surface salinity anomalies of the opposite sign. Both anomalies are advected towards the Ross Sea continental shelf at the respective depths.

7.4 Origin of the temperature anomalies

Tracing the origin of the potential temperature anomalies, model results indicate that these are formed between
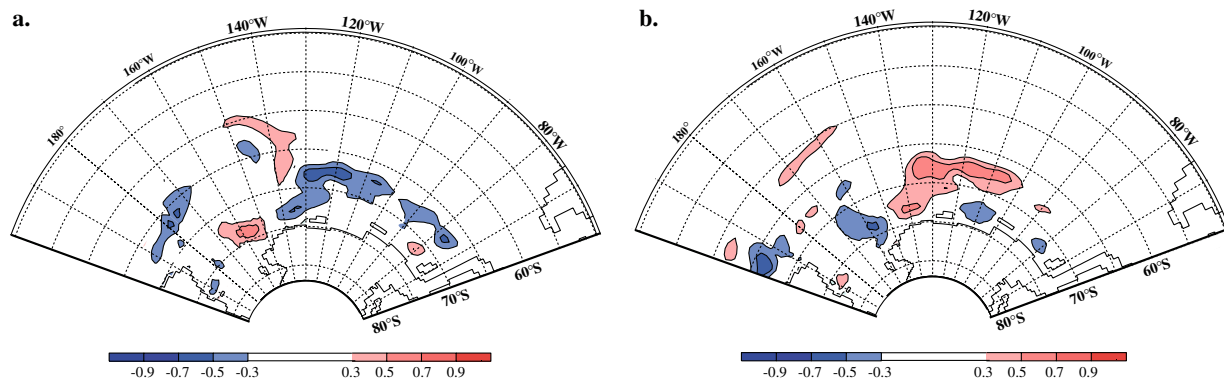
Fig. 18 a Crosscorrelation map between simulated annual means of potential temperature at 400 m and September sea ice growth rates. **b** Crosscorrelation map between annual means of salinity at 150 m and September sea ice growth rates

90°W and 115°W in the eastern Bellingshausen Sea. Here, warm CDW is transported southward along the eastern end of the Ross Gyre extension at 300–2,000 m depth (Fig. 2, 15). Potential temperature anomalies of large amplitude are formed near the coast where warmer CDW and colder shelf waters interact. Potential temperatures at 400 m near the coast in this region are well correlated with the southward transport at this depth with $r = 0.78$ for a lag of 1–2 years (Fig. 19). The lag reflects the low current velocities of 1–2 cm s^{-1} south of the ACC regime.

The faster CDW is transported south towards the western Bellingshausen continental shelf, the less it is cooled and the further south it advects the temperature signal, leading to warm potential temperature anomalies along the continental shelf break. Observed profiles of potential temperature in Pine Island Bay (∼100°W, 74°S), a location known for the exceptionally high melt rates of the bordering glacier, show interannual variability of the order of 1.5°C at depths of 200–400 m between 1992 and 1994 (Jacobs et al. 1996). These observations confirm the magnitude of the temperature anomalies seen in the model (Fig. 13).

Within the coastal current the temperature anomalies travel westward towards the Ross Sea and feed the Antarctic Circumpolar Wave (ACCW) described by Beckmann and Timmermann (2001). The warming peak in the Ross Sea HSSW potential temperature time series can be identified in the time series of Bellingshausen Sea potential temperature anomalies at 400 m with a lag of 8 years (Fig. 19). In combination with an approximate distance of 3,000 km between the Ross and Bellings-

hausen Seas this time lag agrees with current velocities of 1–2 cm s^{-1}. Above 600 m, part of the temperature anomalies also propagate eastward towards the Antarctic Peninsula in agreement with the lag correlation seen in Fig. 14d. At the Antarctic Peninsula the eastward travelling anomalies (Fig. 15) meet the ACCW signal that has surrounded Antarctica in anti-clockwise direction. Since the latter has smaller amplitudes than the signal in the Bellingshausen Sea, this offers an explanation for the cancellation of the ACCW at the Antarctic Peninsula.

8 Discussion and conclusions

We have presented results from a model study of seasonal and interannual variability of HSSW properties in the Ross Sea. Salinity and potential temperature of HSSW formed in the western Ross Sea show oscillatory behaviour at periods of 5–6 and 9 years superimposed on long-term fluctuations. While the shorter oscillations are induced by wind variations, variability on a decadal time scale seems to be related to air temperature fluctuations. A comparison between model results and observations indicates that relatively coarse model resolution and smoothing of the topography result in an overestimation of the MCDW inflow onto the continental shelf. However, model results also suggest that the strong decrease of HSSW salinities deduced from observations (Jacobs et al. 2002) may be an aliasing artefact due to irregular sampling of an oscillatory pattern.

Two processes have previously been proposed as the governing factors for the formation of highly saline shelf waters in the marginal seas of the Southern Ocean. The generally accepted hypothesis assumes that the salinity of dense shelf waters is determined by the amount of brine release due to sea ice formation (e.g. Comiso and Gordon 1998). In a contrasting view Toggweiler and Samuels (1995) propose that the effect of sea ice fresh water fluxes is generally overestimated and that inflow salinities play a role at least as important in the formation of dense shelf waters.

For the Weddell Sea, the existence of a sea-ice related, thermohaline forcing mechanism for the circulation on the continental shelf and in the sub-ice shelf cavities of the Weddell Sea was demonstrated by Timmermann et al. (2002b). Pronounced changes in the regional circulation on the shelf and in the Filchner-Ronne Ice Shelf cavity appear to be caused by changes in the location of the density maximum on the continental shelf, which in turn is linked to fluctuations of sea ice fresh-water fluxes.

For the Ross Sea, the characteristic pattern of a fast northward ice drift and strong brine release in the West and a more sluggish drift of sea ice partially imported from the Amundsen Sea and resulting lower growth rates in the East (Jacobs and Comiso 1989; Assmann et al. 2003) is remarkably steady during the 44-year
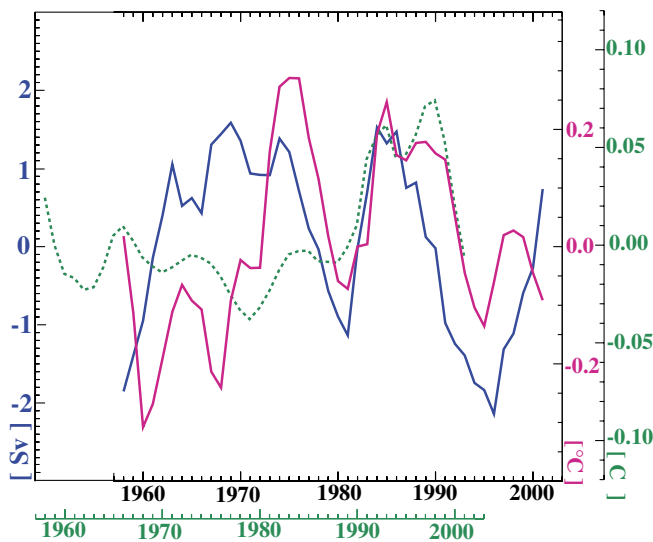
Fig. 19 For the reference simulation: time series of monthly means of the meridional transport anomaly across 68°S between 90°W and 115°W (*blue line*), of the mean potential temperature at 400 m between 90°W and 115°W, south of 68°S (*red line*), and of the mean HSSW potential temperature on the Ross Sea continental shelf (*green dashed line*), all detrended. The latter curve is offset by 8 years (*lower timescale*)

period analysed. The zonal salinity gradient on the Ross Sea continental shelf reflects the gradient in surface fresh-water fluxes, with the density maximum consistently located on the western continental shelf where the Ross Sea polynya is a persistent feature. Its seasonal steepening causes an increase of the transport of the anticyclonic circulation cell that occupies the western shelf and ice shelf cavity (Assmann et al. 2003). Inter-annual variability of the zonal salinity gradient causes a modulation of transport rates, but not of the circulation pattern.

Similar to conditions in the Weddell Sea, the inter-annual variability of sea ice fresh-water fluxes in the western Ross Sea is mainly determined by that of the local atmospheric conditions, particularly by the winds. None of the surface signals, however, can be identified in the simulated variability of HSSW characteristics. Fast advection of surface waters at the time of maximum brine release leads to a strong attenuation of even the seasonal signal towards greater depth. Since the inter-annual variability of surface fresh water fluxes is much smaller than the seasonal signal it cannot penetrate to the bottom. While sea ice formation is responsible for the yearly salinity increase that triggers the formation of HSSW, its variability hardly affects the properties of the resulting water mass.

Instead, results from our model experiments indicate that the signal mainly controling the interannual variability of HSSW characteristics is carried onto the shelf by the inflowing waters. Signals in salinity and potential temperature are hereby found to enter the continental shelf at different depths. The salinity signal is located within sub-surface waters around 150-m depth, while the potential temperature signal is found around 400-m depth within the core of the coastal current.

The origin of the variability of inflow characteristics to the Ross Sea continental shelf can be traced into the Amundsen and Bellingshausen Seas (Fig. 20). In the western Bellingshausen Sea, relatively warm Circumpo-lar Deep Water (CDW) is carried south with the eastern end of the Ross Gyre extension. Fluctuations of the meridional transport induce potential temperature anomalies at the continental shelf break where the CDW interacts with cold shelf waters. This mechanism appears to be the origin of the bottom-intensified potential temperature anomaly within the coastal current that was described as the Antarctic Circumpolar Coastal Wave (ACCW) by Beckmann and Timmermann (2001).

Following the coastal current in about 400 m depth, the temperature anomalies enter the Amundsen Sea. Upwelling due to a persistently cyclonic local wind field carries the signal into the surface mixed layer, leading to fluctuations of the vertical heat flux. Increased vertical heat flux naturally leads to reduced sea ice net freezing rates (and vice versa) and thus causes anomalies of the surface brine input, which eventually creates a sub-surface salinity anomaly. Even in winter convection in this model region does not penetrate below 200 m, so that transmission of the salinity signal is confined to the water column above this level—with the maximum amplitude of variability found at about 150 m depth.

Further downstream, both signals are advected onto the eastern Ross Sea continental shelf. Cooling and salt input due to sea ice formation modifies the properties of the sub-surface waters so that they reach a density that enables them to participate in the formation of HSSW. Convection carries the signal of salinity variability into the deep ocean, where it interacts with relatively warm deep water that features only small variations in salinity but carries the signal of temperature variability and forms the second ingredient of HSSW. Thus, brine input by sea ice formation is neccessary to enable the communication between surface and bottom waters on the continental shelf, but the interannual variability of shelf water characteristics is largely determined by the variability of the shelf inflow induced upstream. We conclude that meridional heat transport in the Amundsen
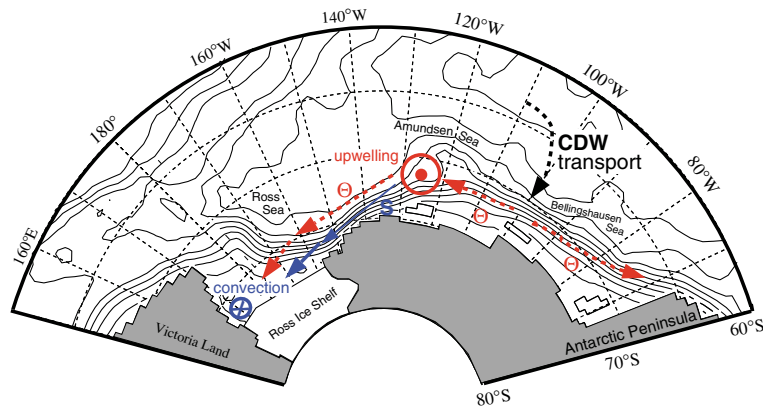
Fig. 20 Map of the Pacific Sector of the Southern Ocean with a schematic representation of the processes relevant to the properties of Ross Sea HSSW. *Blue arrows* denote the propagation of salinity anomalies; red arrows the temperature signals. *Solid lines* refer to sub-surface anomalies; *dashed lines* to transfer in the deep ocean. Bottom topography is represented through isolines of bottom depth. Contour interval is 500 m. *Depth contours* are for orientation only; *arrows* are schematic and not strictly aligned to the appropriate depth contour

and Bellingshausen Seas affects and determines the interannual variability of Ross Sea High Salinity Shelf Water characteristics.

As mentioned above, bottom-intensified anomalies of potential temperatures created on the continental slope of the Amundsen and Bellingshausen Seas travel westward around Antarctica as an Antarctic Circumpolar Coastal Wave (ACCW; Beckmann and Timmermann 2001). Results from our model experiments show that they are joined by salinity anomalies as they leave the Ross Sea. Thus, in agreement with a study by Martinson and Iannuzzi (2003), signals of interannual variability induced in the Pacific sector appear to have an influence on the Weddell Sea. The opposite, however, does not appear to be true. Starting from the source region in the Amundsen and Bellingshausen Seas, an eastward travelling component of the ACCW appears to block or blur signals that propagate westward around the Antarctic Peninsula. The eastward component itself does not seem to affect the inner Weddell Sea, as it is carried northeast with the ACC. Further model studies of the communication paths between the Weddell and Bellingshausen Seas would benefit from a more detailed representation of the passages between the Antarctic Peninsula and the offshore islands.

Naturally, this study leaves some questions unanswered. The driving mechanism of the variability in the southward heat transport associated with the CDW intrusion in the Amundsen and Bellingshausen Seas is still unclear. Although previous research has shown the Amundsen and Bellingshausen Seas to be the main entry for lower latitude variability to the Southern Ocean system (Ledley and Huang 1997; Yuan and Martinson 2000), we cannot identify a clear connection to atmospheric variability.

A second issue is related to the open northern boundary in the model, where a restoring to time-invariant fields of temperature, salinity and vertically integrated transport is prescribed. Sensitivity studies (not shown) suggest a strong link between variations of the ACC transport and the transport of the subpolar gyres, which in nature is likely to introduce additional mechanisms of variability.

Previous oceanographic interest in the Amundsen and Bellingshausen Seas was largely motivated by their ice shelves, which drain a large proportion of the West Antarctic Ice Sheet (Hellmer et al. 1998). With a base below sea level, this ice sheet is particularly vulnerable to climate changes. With all the caveats that are attached to a model study of an issue this complex, this study has shown, however, that oceanic changes in this region also have the potential to strongly affect dense water formation on the Ross Sea continental shelf, and therefore likely the ventilation of the deep Pacific Ocean. Observations of the circulation in the Amundsen and Bellingshausen Seas remain sparse, but in view of the growing evidence of the importance of this region, the data base should be extented despite the logistical difficulties.

References

Assmann KM (2003) The effect of McMurdo Sound topography on water mass exchange across the Ross Ice Shelf front. Annual report of the Filchner-Ronne Ice Shelf Program (FRISP), no. 15. (Available online at http://www.gfi.uib.no/frisp/Rep15/assmann.pdf)

Assmann K, Hellmer HH, Beckmann A (2003) Seasonal variation in circulation and watermass distribution on the Ross Sea continental shelf. Ant Sci 15(1):3–11. DOI:10.1017/S0954102003001007

Baines PG, Condie S (1998) Observations and modelling of Antarctic downslope flows: a review. Antarct Res Ser 75:29–49

Beckmann A, Timmermann R (2001) Circumpolar influences on the Weddell Sea: indication of an Antarctic circumpolar coastal wave. J Climate 14:3785–3792

Beckmann A, Hellmer HH, Timmermann R (1999) A numerical model of the Weddell Sea: large scale circulation and water mass distribution. J Geophys Res 104(C10):23375–23391

Botnikov VN, Chuguy IV (1989) The major features of water circulation and spatial distribution of the Ross Gyral. Polar Geogr Geol 13(3):212–224

Comiso JC, Gordon AL (1998) Interannual variability in summer sea ice minimum, coastal polynyas and bottom water formation in the Weddell Sea. Antarct Res Ser 74:293–315

Fahrbach E, Knoche M, Rohardt G (1991) An estimate of water mass transformation in the southern Weddell Sea. Mar Chem 35:25–44

Fischer H (1995) Vergleichende Untersuchungen eines optimierten dynamisch–thermodynamischen Meereismodells mit Beobachtungen im Weddellmeer [Comparison of an optimized dynamic–thermodynamic sea ice model with observations in the Weddell Sea.]. Berichte zur Polarforschung 166, Alfred-Wegener-Institute, Bremerhaven, 130 pp

Foster TD, Carmack EC (1976) Frontal zone mixing and Antarctic bottom water formation in the southern Weddell Sea. Deep Sea Res 23(4):301–317

Gordon AL, Martinson DG, Taylor HW (1981) The wind-driven circulation in the Weddell-Enderby Basin. Deep Sea Res 28A:151–163

Gouretski VV (1999) The large-scale thermohaline structure of the Ross Gyre. In: Spezie G, Manzella GMR (eds) Oceanography of the Ross Sea. Springer, Berlin Heidelberg New York, pp 77–102

Gouretski V, Jancke K, Reid J, Swift J, Rhines P, Schlitzer R, Yashayaev I (1999) WOCE Hydrographic Programme Special Analysis Centre, Atlas of Ocean Sections CD-ROM, 1999. [Available at http://www.dkrz.de/~u241046/ SACserver/SACHome.htm.]

Greischar LL, Bentley CR, Whiting LR (1992) An analysis of gravity measurements on the Ross Ice Shelf, Antarctica. Antarct Res Ser 57:105–155

Haidvogel DB, Wilkin JL, Young RE (1991) A semi-spectral primitive equation ocean circulation model using vertical sigma and orthogonal curvilinear horizontal coordinates. J Comput Phys 94:151–185

Heap JA (1964) Pack ice Antarctic research. In: Pristley R, Adie R, Robin G (eds) Buterworths, pp 308–317

Hellmer HH, Jacobs SS, Jenkins A (1998) Oceanic erosion of a floating Antarctic glacier in the Amundsen Sea. Antarct Res Ser 75:83–99

Hibler WD (1979) A dynamic-thermodynamic sea ice model. J Phys Oceanogr 9(4):815–846

Jacobs SS, Comiso JC (1989) Sea ice and oceanic processes on the Ross Sea continental shelf. J Geophys Res 94:18195–18211

Jacobs SS, Giulivi CF (1998) Interannual ocean and sea ice variability in the Ross Sea. Antarct Res Ser 75:135–150

Jacobs SS, Amos AF, Bruchhausen PM (1970) Ross sea oceanography and Antarctic bottom water formation. Deep Sea Res 17:935–962

Jacobs SS, Hellmer HH, Jenkins A (1996) Antarctic ice sheet melting in the Southeast Pacific. Geophys Res Lett 23:957–960

Jacobs SS, Giulivi CF, Mele PA (2002) Freshening of the Ross Sea during the late 20th century Science 297:386–389

Jeffries MO, Li S, Jana RA, Krause HR, Hurst-Cushing B (1998) Late winter first-year ice floe variability, seawater flooding and snow ice formation in the Amundsen and Ross Seas. Antarct Res Ser 74:69–88

Johnson MR, Smith AM (1997) Seabed topography under the southern and western Ronne Ice Shelf, derived from seismic surveys. Antarct Sci 9:201–208

Klatt O, Fahrbach E, Hoppema M, Rohardt G (2005) The transport of the Weddell Gyre across the Prime Meridian. Deep-Sea Research (in press)

Ledley TS, Huang Z (1997) A possible ENSO signal in the Ross Sea. Geophys Res Lett 24:3253–3256

Leppäranta M (1983) A growth model for black ice, snow ice, and snow thickness in subantarctic basins. Nord Hydrol 14:59–70

Locarnini RA (1994) Water masses and circulation in the Ross Gyre and environs. PhD Thesis, Texas A & M University, 87 pp

Martinson DG, Iannuzzi RA (2003) Spatial/temporal patterns in Weddell gyre characteristics and their relationship to global climate. J Geophys Res 109(C4). DOI: 10.1029/2000JC000538

Orsi AH, Whitworth T III, Nowlin WD (1995) On the meridional extent and fronts of the Antarctic Circumpolar Current. Deep Sea Res 42:641–673

Owens WB, Lemke P (1990) Sensitivity studies with a sea ice-mixed layer-pycnocline model in the Weddell Sea. J Geophys Res 95(C6):9527–9538

Pacanowski RC, Philander SGH (1981) Parameterization of vertical mixing in numerical models of tropical oceans. J Phys Oceanogr 11:1443–1451

Parkinson CL, Washington WM (1979) A large-scale numerical model of sea ice. J Geophys Res 84(C1):311–337

Reid JL (1986) On the total geostrophic circulation of the South Pacific ocean: flow patterns, tracers and transports. Prog Oceanogr 16:1–61

Semtner AJ Jr (1976) A model for the thermodynamic growth of sea ice in numerical investigations of climate. J Phys Oceanogr 6(3):379–389

Smith WHF, Sandwell DT (1997) Global sea floor topography from satellite altimetry and ship depth soundings. Science 277:1956–1962

Timmermann R, Hellmer HH, Beckmann A (2002b) Simulation of ice-ocean dynamics in the Weddell Sea. Part II: interannual variability 1985–1993. J Geophys Res 107(C3). DOI: 10.1029/2000JC000472

Timmermann R, Beckmann A, Hellmer HH (2002a) Simulation of ice-ocean dynamics in the Weddell Sea. Part I: model configuration and validation. J Geophys Res 107(C3). DOI: 10.1029/2000JC000471

Toggweiler JR, Samuels B (1995) Effect of sea ice on the salinity of Antarctic bottom waters. J Phys Oceanogr 25:1980–1997

Whitworth III T, Peterson RG (1985) The volume transport of the Antarctic circumpolar current from three-year bottom pressure measurements. J Phys Oceanogr 15:810–816

Yuan X, Martinson DG (2000) Antarctic sea ice extent and its global connectivity. J Clim 13:1697–1717